Gemcitabine Mechanism of Action Confounds Early Assessment of Treatment Response by 3'-Deoxy-3'-[18F]Fluorothymidine in Preclinical Models of Lung Cancer

[1] Sonja Schelhaas, [1,*] Annelena Held, [2] Lydia Wachsmuth, [1] Sven Hermann, [3] Davina J. Honess, [3,**] Kathrin Heinzmann, [3] Donna-Michelle Smith, [3] John R. Griffiths, [2] Cornelius Faber, and [1,4] Andreas H. Jacobs

[1] European Institute for Molecular Imaging (EIMI), Westfälische Wilhelms-Universität (WWU) Münster, Münster, Germany

[2] Department of Clinical Radiology, University Hospital of Münster, Münster, Germany

[3] Cancer Research UK Cambridge Institute, Cambridge, UK

[4] Department of Geriatric Medicine, Johanniter Hospital, Bonn, Germany

* present address: Department of Orthopedic Surgery, Otto-von-Guericke University, Magdeburg, Germany

** present address: Comprehensive Cancer Imaging Centre, Imperial College London, UK

running title: [18F]FLT PET and DW-MRI imaging of gemcitabine therapy

key words: [18F]FLT PET, DW-MRI, lung cancer, gemcitabine

corresponding author:

Prof. Dr. med. Andreas H. Jacobs

European Institute for Molecular Imaging (EIMI)

Waldeyerstr. 15

48149 Münster

Germany

Phone: +492518349300

Fax: +492518349313

Email: ahjacobs@uni-muenster.de

conflict of interest: The authors disclose no potential conflicts of interest.

word count: 5000

number of figures: 7

number of tables: 0

number of supplementary figures: 5

number of supplementary tables: 3

ABSTRACT

3'-Deoxy-3'-[^{18}F]fluorothymidine positron emission tomography ([^{18}F]FLT PET) and diffusion weighted magnetic resonance imaging (DW-MRI) are promising approaches to monitor tumor therapy response. Here, we employed these two imaging modalities to evaluate the response of lung carcinoma xenografts in mice after gemcitabine therapy. Caliper measurements revealed that H1975 xenografts responded to gemcitabine treatment, whereas A549 growth was not affected. In both tumor models uptake of [^{18}F]FLT was significantly reduced 6 h after drug administration. Based on the gemcitabine concentration and [^{18}F]FLT excretion measured, this was presumably related to a direct competition of gemcitabine with the radiotracer for cellular uptake. On d1 after therapy [^{18}F]FLT uptake was increased in both models, which was correlated with thymidine kinase 1 (TK1) expression. 2 d and 3 d after drug administration [^{18}F]FLT uptake as well as TK1 and Ki67 expression were unchanged. A reduction in [^{18}F]FLT in the responsive H1975 xenografts could only be noted on d5 of therapy. Changes in ADC$_{mean}$ in A549 xenografts 1 d or 2 d after gemcitabine did not seem to be of therapy-related biological relevance since they were not related to cell death (assessed by caspase-3 immunohistochemistry and cellular density) or tumor therapy response.

Taken together, in these models, early changes of [^{18}F]FLT uptake in tumors reflected mechanisms such as competing gemcitabine uptake or gemcitabine-induced TS inhibition and only reflected growth inhibitory effects at a later time point. Hence, the time point for [^{18}F]FLT PET imaging of tumor response to gemcitabine is of crucial importance.

INTRODUCTION

In anti-cancer therapy many efforts are made to detect response or resistance to treatment at an early time point. This enables an early shift of the therapy regimen, which allows for reduction of side effects, an optimized therapy for the patient, and a reduction of costs for the health care system. Molecular imaging is a valuable tool to non-invasively and longitudinally follow biological and molecular processes within the body. In tumors, these processes may shed light on therapy response. Consequently, use of appropriate imaging biomarkers might help to evaluate anti-cancer therapies in clinical trials. 3'-Deoxy-3'-[^{18}F]fluorothymidine ([^{18}F]FLT) is a radiotracer that is an analog of thymidine, an essential building block of DNA. It is transported into cells in an analogous way to thymidine and is then phosphorylated by thymidine kinase 1 (TK1). The phosphorylated form of [^{18}F]FLT is not incorporated into DNA and the tracer is retained within the cell. Hence, [^{18}F]FLT accumulation is a readout of thymidine salvage pathway activity (1). Positron emission tomography (PET) with [^{18}F]FLT is frequently correlated with cellular markers of proliferation (2) and thus can elucidate the proliferative status of rapidly growing tissue. [^{18}F]FLT PET is beginning to be recognized in the clinic for monitoring response to anti-cancer agents (3) since reductions in proliferation occur prior to reductions in tumor volume, which can be assessed by anatomical imaging modalities like computed tomography (CT) or magnetic resonance imaging (MRI). MRI is also capable of detecting changes of the tissue composition within tumors. Diffusion weighted (DW)-MRI sensitively depicts micro-structural reorganizations due to cell swelling and shrinkage. An increase of the apparent diffusion coefficient (ADC) reflects cell death induced loss of membrane integrity and a relative increase of the extracellular space (4,5).

Gemcitabine (2′,2′-difluorodeoxycytidine, dFdC) is a chemotherapeutic agent employed in e.g. lung (6) or pancreatic cancer (7). It exerts an anti-cancer effect

mostly by interfering with DNA synthesis. Its metabolites can be incorporated into DNA, thereby abrogating effective DNA synthesis. Furthermore, it inhibits thymidylate synthase (TS), the key enzyme of the thymidine *de novo* synthesis pathway (8,9). This pathway is the alternative pathway to the thymidine salvage pathway which is the basis for [18F]FLT uptake in tissues. It has been shown for other TS-inhibiting agents, that a counter-mechanistic upregulation of the salvage pathway results in increased uptake of [18F]FLT (10,11).

Here, we investigate whether [18F]FLT PET and DW-MRI are suitable methods to detect gemcitabine-induced therapy response in experimental lung cancer xenograft models by employing a gemcitabine-sensitive and an -insensitive lung cancer model.

MATERIALS AND METHODS

Cell culture experiments

A549 (DSMZ) and H1975 (LGC standards, both obtained in 12/2011) non-small cell lung cancer cells were cultured at 37 °C in 5 % CO_2 with DMEM or RPMI, respectively, containing 10 % fetal calf serum, 100 U/mL penicillin and 100 µg/mL streptomycin. Cell line identity was confirmed by the supplier by short tandem repeat analysis and cells were used at early passage. An MTT assay (Sigma, M5655) was performed according to the manufacturer's protocol to determine cell viability after gemcitabine administration. Cells were incubated for 48 h with different concentrations of gemcitabine (0.01 µM – 10 µM, Gemzar, Eli Lilly, obtained from the pharmacy of the University Hospital Münster).

For *in vitro* [^{18}F]FLT uptake assays 1.5×10^5 cells/well were seeded in 6-well plates 72 h prior to the experiment. 0.5 µM, 1 µM or 10 µM gemcitabine were added 4 h, 24 h or 48 h before medium was exchanged for 1 h for medium containing 0.142 MBq/mL [^{18}F]FLT. After three washing steps, cells were detached, and tracer uptake was determined in a 2480 automatic Gamma Counter "Wallac Wizzard2 3'' (Perkin Elmer). Cell number was assessed in a Z2 coulter particle count and size analyser (Beckman Coulter). To measure competition between [^{18}F]FLT and gemcitabine *in vitro*, 5×10^5 cells were seeded the day before the experiment. Cells were incubated with the indicated concentrations of the drug for 1 h or 4 h and then incubated with [^{18}F]FLT either in the presence (+) or absence (-) of gemcitabine. Tracer uptake was determined as described above.

Western blot

Cells were lysed in RIPA and subjected to polyacrylamide gel electrophoresis. After transfer to a PVDF membrane, proteins were probed with antibodies targeting TK1 (Abcam, EPR3193, 1:1000) or actin (MP Biomedicals, clone C4, 69100, 1:1000). Secondary antibodies were coupled with peroxidase, and signals were visualized with Pierce ECL Plus Western Blotting Substrate (Pierce Biotechnology). Densitometry analysis of bands was performed with ImageJ and plotted relative to actin loading control. TK1 expression levels were normalized to the expression of NaCl treated control cells on the same blot.

Animal Model

Animal procedures were performed within the multi-center QuIC-ConCePT study in accordance with the German Laws for Animal Protection and were approved by the animal care committee of the local government (North Rhine-Westphalia State Agency for Nature, Environment and Consumer Protection). During the experiments general health and body weight of the mice were monitored. 6-8 week old female NMRI nude mice (Janvier Labs) were used for the experiments. Three tumors per mouse were inoculated subcutaneously in the shoulder region by injection of 2×10^6 cells in 50 µL medium. Tumor volumes were calculated from digital caliper measurements (volume = $\pi/6 \times (L \times W^2)$; L: longer diameter, W: shorter diameter). Mice were treated by intraperitoneal injection of 100 mg/kg gemcitabine in 100 µL 0.9 % NaCl at 3 d intervals or 0.9 % NaCl as control. Imaging was performed according to the experimental schedule depicted in **Supplementary Fig. S1**.

PET imaging

[^{18}F]FLT was produced with purity of >99 % as reported previously (12). Mice were anesthetized with isoflurane inhalation (2 % in oxygen), and temperature was maintained at 37 °C by using a heating pad. 10 MBq of radiotracer were injected intravenously and image acquisition was performed for 20 min after a 70 min tracer uptake period using a quadHIDAC small animal PET scanner (Oxford Positron Systems (13)). A multimodal bed was used to enable co-registration of PET images with anatomical images from CT (Inveon, Siemens Medical Solutions) or T2w MRI. Images were analyzed with the software Inveon Research Workplace 3.0 (Siemens Medical Solutions). Three-dimensional volumes-of-interest (VOIs) were defined on CT or MR images over the entire tumor. Radiotracer uptake was calculated as maximal percentage injected dose per mL ($\%ID_{max}/mL$). In addition, we also determined $\%ID_{mean}/mL$, standardized uptake value (SUV_{max}, SUV_{mean}), and maximal tumor-to-muscle$_{mean}$ and tumor-to-liver$_{mean}$-ratio. Results of the mean tumor uptake were substantially influenced by necrosis within the tumors. We also assessed the 25%ile, representing the mean of the 25% highest intensity voxels. All additional evaluations are listed in **Supplementary Table S1**, and were used to demonstrate that findings were independent of the mode of data analysis To evaluate relative excretion, the radioactivity within the bladder VOI ($\%ID_{mean}/mL$) was multiplied by the volume of the VOI and divided by the total radioactivity within the mouse.

MR imaging

T2 weighted (T2w) MR images were obtained with a 9.4 T Bruker Biospec (2D rapid acquisition with relaxation enhancement, repetition / echo time (TR/TE) 3600/40 ms, Rare factor 8, field of view (FOV) 35 mm, 256 matrix, slice thickness 1 mm) to obtain anatomical information for the definition of VOIs. ADC was determined by DW-MRI (EPI-DTI, TR/TE 1000/19 ms, 12 segments, effective b-values = 2, 54, 109, 204, 309,

413, 620, 702 s/mm², FOV 35 mm, 128 matrix, NEX 6, respiration-triggered, slice thickness 1 mm, 4 slices in the tumor center). ADC maps were calculated with the software ParaVision 5.1 (monoexponential fit of all b-values). ImageJ (National Institutes of Health) was employed to manually segment the tumors in ADC maps and determine the ADC_{mean} of up to 4 slices per tumor.

Immunohistochemistry

Tumors were fixed in 4 % paraformaldehyde and embedded in paraffin. Transverse 5 µm sections were incubated overnight at 4 °C with primary antibodies (Ki67: Abcam, ab 16667, 1:100; TK1: Abcam, EPR3193, 1:200) and for 1 h at room temperature with respective biotin or fluorescently labeled secondary antibodies. Staining was evaluated using a Nikon Eclipse 90i fluorescent microscope and the NIS-Elements software package (Nikon). For quantification five images at 20x resolution were acquired in regions with the highest fraction of specifically stained cells to compare the labeling to radiotracer uptake expressed as $\%ID_{max}/mL$. For Ki67 stained nuclei relative to the total number of DAPI stained nuclei were determined. For TK1 the staining positive area was evaluated after color deconvolution with ImageJ.

Thymidine and gemcitabine quantification

Thymidine was analyzed with a modified liquid-chromatography-mass spectrometry (LC-MS/MS) method as described previously (14). Gemcitabine LC-MS/MS was performed according to Bapiro et al. (15).

Statistics

Data are displayed as box plots showing median values with 25 % and 75 %

percentiles, with whiskers from minimum to maximum. Means ± standard deviation are listed in the **Supplementary Table S2.** The numbers in brackets indicate the number of samples analyzed. SigmaPlot 13.0 was used for statistical analyses. Since not all data followed a normal distribution the Mann-Whitney Rank Sum Test was applied for comparisons. IC_{50} values were determined using the standard curve macro. Correlations were calculated with the Pearson method. *P* values < 0.05 were considered statistically significant.

RESULTS

Incubation of H1975 or A549 tumor cells with gemcitabine results in cell death and induction of increased [^{18}F]FLT uptake *in vitro*

We previously determined that H1975 and A549 lung cancer xenografts accumulate [^{18}F]FLT and therefore should be suitable to monitor treatment efficacy (16). MTT assays revealed similar half maximum inhibitory concentrations of these two cell lines *in vitro* (IC$_{50}$[H1975] = 0.33 µM ± 0.19 µM, *n* = 6, IC$_{50}$[A549] = 0.79 µM ± 0.26 µM, *n* = 4, *P* < 0.05). Thus, both cell lines were responsive to gemcitabine therapy. We performed [^{18}F]FLT uptake assays *in vitro* to assess whether gemcitabine induces changes in tracer uptake under such conditions (**Fig. 1A**). No differences in [^{18}F]FLT accumulation were apparent after 4 h incubation with the drug. After 24 h and 48 h, [^{18}F]FLT accumulation was significantly increased in H1975 cells. A similar pattern was observed in gemcitabine treated A549 cells. However, longer exposure times induced a higher rate of cell death in A549 cells (**Fig. 1B**), which was accompanied by reduced tracer uptake in this experimental setup. Gemcitabine incubation was accompanied by increased TK1 expression as determined by western blot (**Fig. 1C**). Thus, a TK1-associated increase in [^{18}F]FLT uptake was noted in both cell lines within 24 h, followed by a drug-dose dependent decrease in A549 cells.

In *vivo* growth of H1975 is affected by gemcitabine therapy whereas A549 growth is unaltered

We gave four doses of 100 mg/kg gemcitabine to nude mice bearing subcutaneous H1975 or A549 xenografts of a size of about 100 mm^3. A549 xenografts grew substantially more slowly. There was no evidence of gemcitabine-induced toxicity. A growth inhibitory effect was observed from d5 onwards for H1975 xenografts (**Fig. 2A**), whereas growth of A549 was unaffected (**Fig. 2B**). Thus, a gemcitabine-

responsive and a non-responsive model were available to evaluate the ability of [^{18}F]FLT PET and DW-MRI to detect any effects of gemcitabine treatment on the tumors.

Gemcitabine affects [^{18}F]FLT uptake in both models *in vivo*

We performed [^{18}F]FLT PET imaging at various time points after administration of gemcitabine (**Fig. 3**). In both tumor types tracer uptake was significantly reduced within hours after drug application and significantly increased on d1 (%ID$_{max}$/mL of H1975: baseline: 18.6 ± 3.3, 6 h: 9.8 ± 2.0, $P < 0.001$; d1: 21.5 ± 3.2, $P < 0.01$; A549: baseline: 6.39 ± 1.57, 6 h: 3.68 ± 0.68, $P < 0.001$; d1: 8.95 ± 2.75, $P < 0.001$, significances relative to baseline, see **Supplementary Table S2** for all numbers). On d2 and d3 [^{18}F]FLT uptake was equal to baseline and to respective NaCl controls. A significant reduction in [^{18}F]FLT uptake could be noted in H1975 xenografts on d5 of gemcitabine therapy (15.0 ± 3.4, $P < 0.01$ relative to baseline). In contrast to all other observations, the slight increase of [^{18}F]FLT uptake in H1975 tumors on d2 and in A549 xenografts on d5 could not be confirmed with most other [^{18}F]FLT uptake parameters (see **Supplementary Table S1**).

We analyzed Ki67 immunohistochemistry to assess whether [^{18}F]FLT accumulation reflects cellular proliferation. In both tumor models, Ki67 was unchanged after gemcitabine therapy (**Fig. 4** and **Supplementary Fig.S2**). Unaltered [^{18}F]FLT on d2 and d3 was in accordance with unchanged cellular proliferation as determined by Ki67 immunohistochemistry. The cause for the above described changes in [^{18}F]FLT uptake (i.e. decrease after 6 h, increase after 1 d, and decrease after 5 d in H1975 xenografts) appeared to be unrelated to this proliferation marker.

Immunohistochemical analysis revealed an increased TK1 expression on d1 after gemcitabine (% positive area of H1975: NaCl: 21.5 ± 5.0, d1: 45.1 ± 8.8; A549: NaCl: 19.9 ± 5.8, d1: 36.8 ± 4.3; both $P < 0.01$ relative to NaCl control). A significant positive correlation of TK1 expression and [^{18}F]FLT uptake was measured in both models (**Fig. 5**). Of note, for the H1975 tumors, PET imaging after 6 h was only performed in longitudinal studies. Hence, immunohistochemistry at this time point was conducted in a different cohort of mice, not allowing direct correlation analysis of this time point. For consistency, we did not plot this time point for A549 either; however, inclusion of these 6 h data also results in a significant correlation of [^{18}F]FLT uptake and TK1 expression ($r = 0.539$, $P < 0.01$).

 [^{18}F]FLT uptake after 6 h in tumors was low although TK1 expression was elevated. Also TS or human equilibrative nucleoside transporter 1 (hENT1) expression analysis did not explain reduced [^{18}F]FLT (**Supplementary Fig. S3**). Interestingly, not only tumor uptake was reduced at this time point but [^{18}F]FLT retention in a range of other organs was also diminished (e.g. spleen, muscle or lymph nodes, see **Supplementary Table S3**), indicating a potential systemic rather than a tumor-specific effect. Gemcitabine, being a nucleoside analog, employs cellular transport mechanisms similar to the ones used by [^{18}F]FLT and thymidine. Hence, we hypothesized that high gemcitabine concentrations in the plasma compete with [^{18}F]FLT for cellular uptake.

We showed that less [^{18}F]FLT is taken up by cells in the presence of gemcitabine *in vitro* (**Fig. 6A**), confirming the competitive nature of these two molecules. *In vivo*, LC-MS/MS analysis revealed gemcitabine (dFdC) tumor concentrations of 3.38 µM ± 2.34 µM in H1975 ($n = 4$) and ~1.2 µM in A549 ($n = 2$) and plasma concentrations in the range of 0.16 µM ± 0.08 µM ($n = 5$) 6 h after drug administration. The latter is well

above concentrations estimated for $[^{18}F]FLT$ (~ 0.01 µM) and could effectively reduce the amount of $[^{18}F]FLT$ taken up by cells. Consequently, since less $[^{18}F]FLT$ was taken up and retained in cells throughout the body, more tracer should be excreted. By quantifying the amount of tracer within the bladder, we showed that more $[^{18}F]FLT$ was excreted 6 h after gemcitabine administration (% $[^{18}F]FLT$ in bladder: baseline: 13.7 ± 5.8, 6 h: 24.8 ± 6.5, $P < 0.05$, **Fig. 6B**). Thymidine also employs the cellular uptake mechanism for nucleosides. Plasma concentration of thymidine was significantly higher at 6 h (**Fig. 6C**). Based on its short half-life (~30 min (17,18)), plasma gemcitabine concentrations should be in the range of ~500 µM immediately after drug administration. This ~500-fold excess of gemcitabine over plasma thymidine suggests that increased thymidine concentrations after 6 h result from competition with gemcitabine. At later time points, plasma thymidine levels were significantly reduced relative to NaCl control whereas thymidine concentrations within H1975 tumors were increased (**Fig. 6D**).

ADC is slightly altered early after gemcitabine administration

We also determined whether gemcitabine application causes changes in the apparent diffusion coefficient (ADC), the measure for water diffusivity as determined by DW-MRI. **Fig. 7A** shows that ADC_{mean} did not vary substantially on d1 or d2 after treatment in H1975 xenografts. In A549 tumors a small increase in ADC relative to baseline was detected, which was independent of treatment. This increase was more pronounced 1 d after gemcitabine. However, in both models, cellular density (**Fig. 7B**) and cell death (cleaved caspase-3 immunohistochemistry, **Supplementary Fig. S4**) were not altered at these time points.

DISCUSSION

We employed two lung cancer models to investigate the effect of gemcitabine on [^{18}F]FLT PET and DW-MRI. The two models differed with respect to gemcitabine sensitivity *in vivo*. We observed a growth inhibition-related decrease of [^{18}F]FLT uptake on d5 of treatment in the sensitive H1975 xenografts. Early changes in tracer uptake (within hours and on d1), as well as ADC, were not related to treatment response. These results indicate that a detailed understanding of the various mechanisms determining changes in imaging biomarkers is important when interpreting such changes for the analysis of therapy response, especially at early time points. With regards to gemcitabine, the mechanisms influencing [^{18}F]FLT uptake are rather complex, as elucidated here.

There is a range of studies describing the successful use of [^{18}F]FLT PET for predicting response to anti-cancer agents (19,20). When employing agents interfering with TS activity, like 5-FU, an increase in [^{18}F]FLT uptake early after drug administration was frequently reported. This effect has been attributed either to upregulation of TK1 activity (10,11) or to redistribution of hENT1 to the cellular surface (21).

Gemcitabine also inhibits TS activity (8). Consequentially, we also observed an [^{18}F]FLT increase both *in vitro* (**Fig. 1**) and *in vivo* (**Fig. 3**). This is in accordance with an *in vitro* study that reported a 5-fold increase of [^{18}F]FLT 24 h after treatment with gemcitabine in oesophageal squamous cell carcinoma cells (22). In our models, we showed that increased [^{18}F]FLT was related to TK1 expression (**Fig. 1C and Fig. 5**).

We noted a substantial decrease of tumor [^{18}F]FLT accumulation 6 h after gemcitabine administration (**Fig. 3**). This reduction was not related to expression of Ki67, TK1, TS or hENT1. Our *in vivo* data indicate that competition of gemcitabine

uptake with [^{18}F]FLT is most likely the cause for the reduced [^{18}F]FLT uptake, as also demonstrated by *in vitro* [^{18}F]FLT uptake experiments (**Fig. 6A**). Both molecules share cellular uptake mechanisms, and the major transporter is presumably hENT1. Expression of hENT1 predicts gemcitabine response in patients with biliary tract cancer (23), cholangiocarcinoma (24) or pancreatic cancer (25). Furthermore, Paproski et al. demonstrated that [^{3}H]FLT uptake predicts transport and toxicity of gemcitabine in a range of pancreatic cancer cell lines *in vitro* (26).

We determined gemcitabine plasma concentrations to be ~160 nM about 6 h after drug application. This is in good agreement with previously published gemcitabine concentrations (15,27). According to Zhang et al., the estimated dose level of [^{18}F]FLT used in preclinical imaging is 2 µg/kg (8.2 nM) (28), resulting in competition of [^{18}F]FLT and gemcitabine for cellular transport mechanisms which could be measured by PET and gamma counter measurements in our study.

We showed that less [^{18}F]FLT accumulated in a range of organs 6 h after gemcitabine administration because less tracer was taken up by the cells. Hence, more [^{18}F]FLT would be excreted and indeed the amount of [^{18}F]FLT in the bladder increased by about 70 % (**Fig. 6B**). One might speculate that such a systemic effect on tracer uptake calls for correction of [^{18}F]FLT uptake to an internal reference tissue. But after also correcting for muscle or liver uptake, the relative decrease in tumor [^{18}F]FLT accumulation remained significant (**Supplementary Table S1**). This implies that gemcitabine is preferentially taken up in tumors, in agreement with a study demonstrating a 3.5-fold increased accumulation of gemcitabine relative to liver (18). Hence, there are multiple pieces of evidence that support the hypothesis that 6 h after administration gemcitabine competes with [^{18}F]FLT for cellular uptake.

We also observed competition of gemcitabine with plasma thymidine 6 h after drug administration (**Fig. 6C**). d1, d2 and d3 after gemcitabine, plasma thymidine

concentrations were reduced relative to the NaCl control. This is in line with other studies employing TS-inhibiting agents which showed reduced thymidine levels in plasma in mice (29) and men (30), presumably originating from the drug induced blockade of the *de novo* pathway and increased use of the salvage pathway and hence extracellular thymidine. A significant increase in thymidine concentration was noted in H1975 xenografts. This could possibly be caused by an accumulation of phosphorylated thymidine within the cells, which cannot be incorporated into the DNA since gemcitabine inhibits DNA synthesis. The fact that this increase in thymidine cannot be detected in A549 xenografts, whose growth is not impaired after gemcitabine treatment, supports this hypothesis.

Of note, changes in [^{18}F]FLT uptake and TK1 expression within the first days were observed in both tumor models investigated, even though they substantially differed with respect to sensitivity to gemcitabine (**Fig. 2**). Gemcitabine concentrations within A549 tumors were in a similar range to those in H1975 tumors, demonstrating that gemcitabine is capable of entering these cells. A double dose of gemcitabine did cause a reduction in tumor volume in a small cohort of mice (**Supplementary Fig. S5**). Hence, as previously reported (31,32), A549 xenografts were not intrinsically resistant to this drug, but in our study the dose used was sub-therapeutic. Consequently, the observed early changes in [^{18}F]FLT uptake (reduction after 6 h and increase after 1 d) were not related to treatment response. This is in accordance with studies showing that sub-therapeutic doses of TS inhibiting agents induce an [^{18}F]FLT increase *in vitro* (33) and *in vivo* (34).

A growth inhibition-related decrease in [^{18}F]FLT uptake was only seen on d5 of gemcitabine therapy. Presumably, this was related to increased apoptosis as determined by immunohistochemistry of cleaved caspase-3 (**Supplementary Fig.**

S4). In our study, H1975 tumor volumes between the treated and the untreated groups were already significantly different on d5. Hence, molecular imaging with [^{18}F]FLT PET would not provide additional (earlier) information over volume measurements. However, findings on timing from preclinical studies cannot be directly transferred to the clinical situation. In general, clinical tumors grow more slowly than preclinical xenografts. This could result in reductions in [^{18}F]FLT occurring prior to reductions in tumor volume. Consequently, [^{18}F]FLT PET could potentially be used for the assessment of treatment response in cancer patients treated with gemcitabine, if imaging is not performed within the first days of therapy. Moreover, a detailed kinetic analysis deciphering [^{18}F]FLT delivery and transport (K1) from the rate of phosphorylation (k3) could be envisioned to especially shed light into gemcitabine action on [^{18}F]FLT metabolism in clinical applications.

In our study, results were obtained from mice bearing several tumors. The advantage of this model system is, that according to the principles of the 3Rs (replacement, reduction, refinement) the number of animals can be reduced. Most importantly, the tracer input function is the same for tumors growing in the same animal. Therefore, differences in [^{18}F]FLT uptake can be attributed to differences in tumor growth (location, vascularization, biologic activity) and not to potential differences in the imaging protocol. However, one has to bear in mind, that analyses of mice bearing single xenografts could potentially better reflect the clinical situation with its interindividual biological heterogeneities.

DW-MRI is an alternative imaging approach to monitor cancer therapy, as has been shown e.g. for experimental Ewing sarcoma (35). We were unable to detect any substantial differences in tumor ADC$_{mean}$ 1 d or 2 d after a single dose of gemcitabine in either of the lung tumor models investigated here (**Fig. 7A**). This was in

accordance with unchanged cellular density and cell death. The slight increase in ADC in A549 xenografts most likely resulted from other structural changes such as a growth-related increase in necrosis, which was irrespective of treatment. These observations emphasize that ADC is a versatile measure that is influenced by a complex combination of parameters related to tissue micro-structure. Transient effects such as cell swelling or shrinkage possibly overshadow changes of parameters that can be related to therapy with our current knowledge. Hence, in our model ADC had no predictive value.

In conclusion, our data demonstrate that plasma levels of gemcitabine alter nucleoside transporter availability and hence [18F]FLT uptake early after gemcitabine administration. Moreover, molecular factors like TK1 activity might hamper the straightforward non-invasive detection of early treatment effects by [18F]FLT PET when employing agents inhibiting TS. Hence, understanding the mechanism of action of a therapeutic approach as well as the mechanisms of [18F]FLT uptake are crucial for interpreting respective PET imaging findings.

REFERENCES

1. Been LB, Suurmeijer AJH, Cobben DCP, Jager PL, Hoekstra HJ, Elsinga PH. [18F]FLT-PET in oncology: current status and opportunities. Eur J Nucl Med Mol Imaging. 2004;31:1659–72.

2. Chalkidou A, Landau DB, Odell EW, Cornelius VR, O'Doherty MJ, Marsden PK. Correlation between Ki-67 immunohistochemistry and 18F-fluorothymidine uptake in patients with cancer: A systematic review and meta-analysis. Eur J Cancer. 2012;48:3499–513.

3. Soloviev D, Lewis D, Honess D, Aboagye E. [(18)F]FLT: an imaging biomarker of tumour proliferation for assessment of tumour response to treatment. Eur J Cancer. England; 2012;48:416–24.

4. Sinkus R, Van Beers BE, Vilgrain V, DeSouza N, Waterton JC. Apparent diffusion coefficient from magnetic resonance imaging as a biomarker in oncology drug development. Eur J Cancer. 2012;48:425–31.

5. Le Bihan D, Iima M. Diffusion Magnetic Resonance Imaging: What Water Tells Us about Biological Tissues. PLoS Biol. 2015;13:e1002203.

6. Reynolds JK, Levien TL. Quality-of-life assessment in phase III clinical trials of gemcitabine in non-small-cell lung cancer. Drugs Aging. 2008;25:893–911.

7. de Sousa Cavalcante L, Monteiro G. Gemcitabine: metabolism and molecular mechanisms of action, sensitivity and chemoresistance in pancreatic cancer. Eur J Pharmacol. 2014;741:8–16.

8. Honeywell RJ, Ruiz van Haperen VWT, Veerman G, Smid K, Peters GJ. Inhibition of thymidylate synthase by 2',2'-difluoro-2'-deoxycytidine (Gemcitabine) and its metabolite 2',2'-difluoro-2'-deoxyuridine. Int J Biochem Cell Biol. 2015;60:73–81.

9. Mini E, Nobili S, Caciagli B, Landini I, Mazzei T. Cellular pharmacology of gemcitabine. Ann Oncol. 2006;17 Suppl 5:v7–12.

10. Lee SJ, Kim SY, Chung JH, Oh SJ, Ryu JS, Hong YS, et al. Induction of thymidine kinase 1 after 5-fluorouracil as a mechanism for 3'-deoxy-3'-[18F]fluorothymidine flare. Biochem Pharmacol. 2010;80:1528–36.

11. Hong IK, Kim SY, Chung JH, Lee SJ, Oh SJ, Lee SJ, et al. 3'-Deoxy-3'-[18F]fluorothymidine positron emission tomography imaging of thymidine kinase 1 activity after 5-fluorouracil treatment in a mouse tumor model. Anticancer Res. 2014;34:759–66.

12. Viel T, Schelhaas S, Wagner S, Wachsmuth L, Schwegmann K, Kuhlmann M, et al. Early assessment of the efficacy of temozolomide chemotherapy in experimental glioblastoma using [18F]FLT-PET imaging. PLoS One. 2013;8:e67911.

13. Schäfers KP, Reader AJ, Kriens M, Knoess C, Schober O, Schäfers M. Performance evaluation of the 32-module quadHIDAC small-animal PET scanner. J Nucl Med. 2005;46:996–1004.

14. Heinzmann K, Honess DJ, Lewis DY, Smith D-M, Cawthorne C, Keen H, et al. The relationship between endogenous thymidine concentrations and [(18)F]FLT uptake in a range of preclinical tumour models. EJNMMI Res. 2016;6:63.

15. Bapiro TE, Richards FM, Goldgraben MA, Olive KP, Madhu B, Frese KK, et al. A novel method for quantification of gemcitabine and its metabolites 2',2'-difluorodeoxyuridine and gemcitabine triphosphate in tumour tissue by LC-MS/MS: comparison with (19)F NMR spectroscopy. Cancer Chemother Pharmacol. 2011;68:1243–53.

16. Schelhaas S, Wachsmuth L, Viel T, Honess DJ, Heinzmann K, Smith D-M, et

al. Variability of proliferation and diffusion in different lung cancer models as measured by 3'-deoxy-3'-18F-fluorothymidine PET and diffusion-weighted MR imaging. J Nucl Med. 2014;55:983–8.

17. Veerman G, Ruiz van Haperen VW, Vermorken JB, Noordhuis P, Braakhuis BJ, Pinedo HM, et al. Antitumor activity of prolonged as compared with bolus administration of 2',2'-difluorodeoxycytidine in vivo against murine colon tumors. Cancer Chemother Pharmacol. 1996;38:335–42.

18. Wang H, Li M, Rinehart JJ, Zhang R. Pretreatment with Dexamethasone Increases Antitumor Activity of Carboplatin and Gemcitabine in Mice Bearing Human Cancer Xenografts: In Vivo Activity, Pharmacokinetics, and Clinical Implications for Cancer Chemotherapy. Clin Cancer Res. 2004;10:1633–44.

19. Jensen MM, Kjaer A. Monitoring of anti-cancer treatment with (18)F-FDG and (18)F-FLT PET: a comprehensive review of pre-clinical studies. Am J Nucl Med Mol Imaging. 2015;5:431–56.

20. Schelhaas S, Heinzmann K, Bollineni VR, Kramer GM, Liu Y, Waterton JC, et al. Preclinical Applications of 3'-Deoxy-3'-[18F]Fluorothymidine in Oncology – A Systematic Review. Theranostics. 2016;in press.

21. Perumal M, Pillai RG, Barthel H, Leyton J, Latigo JR, Forster M, et al. Redistribution of nucleoside transporters to the cell membrane provides a novel approach for imaging thymidylate synthase inhibition by positron emission tomography. Cancer Res. 2006;66:8558–64.

22. Dittmann H, Dohmen BM, Kehlbach R, Bartusek G, Pritzkow M, Sarbia M, et al. Early changes in [18F]FLT uptake after chemotherapy: an experimental study. Eur J Nucl Med Mol Imaging. 2002;29:1462–9.

23. Santini D, Schiavon G, Vincenzi B, Cass CE, Vasile E, Manazza AD, et al. Human equilibrative nucleoside transporter 1 (hENT1) levels predict response to gemcitabine in patients with biliary tract cancer (BTC). Curr Cancer Drug Targets. 2011;11:123–9.

24. Borbath I, Verbrugghe L, Lai R, Gigot JF, Humblet Y, Piessevaux H, et al. Human equilibrative nucleoside transporter 1 (hENT1) expression is a potential predictive tool for response to gemcitabine in patients with advanced cholangiocarcinoma. Eur J Cancer. 2012;48:990–6.

25. Greenhalf W, Ghaneh P, Neoptolemos JP, Palmer DH, Cox TF, Lamb RF, et al. Pancreatic cancer hENT1 expression and survival from gemcitabine in patients from the ESPAC-3 trial. J Natl Cancer Inst. 2014;106:djt347.

26. Paproski RJ, Young JD, Cass CE. Predicting gemcitabine transport and toxicity in human pancreatic cancer cell lines with the positron emission tomography tracer 3'-deoxy-3'-fluorothymidine. Biochem Pharmacol. 2010;79:587–95.

27. Awasthi N, Zhang C, Schwarz AM, Hinz S, Wang C, Williams NS, et al. Comparative benefits of Nab-paclitaxel over gemcitabine or polysorbate-based docetaxel in experimental pancreatic cancer. Carcinogenesis. 2013;34:2361–9.

28. Zhang CC, Yan Z, Li W, Kuszpit K, Painter CL, Zhang Q, et al. [(18)F]FLT-PET imaging does not always "light up" proliferating tumor cells. Clin Cancer Res. 2012;18:1303–12.

29. Clarke SJ, Farrugia DC, Aherne GW, Pritchard DM, Benstead J, Jackman AL. Balb/c mice as a preclinical model for raltitrexed-induced gastrointestinal toxicity. Clin Cancer Res. 2000;6:285–96.

30. Li KM, Rivory LP, Hoskins J, Sharma R, Clarke SJ. Altered deoxyuridine and thymidine in plasma following capecitabine treatment in colorectal cancer patients. Br J Clin Pharmacol. 2007;63:67–74.

31. Kim I-Y, Kang Y-S, Lee DS, Park H-J, Choi E-K, Oh Y-K, et al. Antitumor activity of EGFR targeted pH-sensitive immunoliposomes encapsulating gemcitabine in A549 xenograft nude mice. J Control Release. 2009;140:55–60.

32. Zundelevich A, Elad-Sfadia G, Haklai R, Kloog Y. Suppression of lung cancer tumor growth in a nude mouse model by the Ras inhibitor salirasib (farnesylthiosalicylic acid). Mol Cancer Ther. 2007;6:1765–73.

33. Yau K, Price P, Pillai RG, Aboagye E. Elevation of radiolabelled thymidine uptake in RIF-1 fibrosarcoma and HT29 colon adenocarcinoma cells after treatment with thymidylate synthase inhibitors. Eur J Nucl Med Mol Imaging. 2006;33:981–7.

34. Viertl D, Bischof Delaloye A, Lanz B, Poitry-Yamate C, Gruetter R, Mlynarik V, et al. Increase of [(18)F]FLT tumor uptake in vivo mediated by FdUrd: toward improving cell proliferation positron emission tomography. Mol imaging Biol. 2011;13:321–31.

35. Reichardt W, Juettner E, Uhl M, Elverfeldt D V, Kontny U. Diffusion-weighted imaging as predictor of therapy response in an animal model of Ewing sarcoma. Invest Radiol. 2009;44:298–303.

FIGURE LEGENDS

Figure 1. Gemcitabine induced an increase in uptake of [^{18}F]FLT in H1975 and A549 tumor cells *in vitro*. (A) [^{18}F]FLT uptake assays revealed elevated radiotracer retention after prolonged treatment with gemcitabine in both cell lines. Tracer accumulation is expressed as counts per minute (cpm) per cell. (B) Cell number is displayed as an indicator of cell viability after gemcitabine therapy. Boxplots depict medians of six values obtained in three individual experiments. (C) Western blot analysis of cell lysates revealed increased expression of TK1 after gemcitabine treatment. $n = 4$ samples were analyzed per condition. *: $P < 0.05$; **: $P < 0.01$ relative to NaCl control.

Figure 2. Gemcitabine therapy induced growth inhibition in H1975 but not in A549 xenografts. Tumor volumes were determined by caliper measurements and showed a growth inhibitory effect of gemcitabine (given on d0, d3, d6, and d9) in H1975 but not in A549 tumors. White: NaCl; grey: gemcitabine; *: $P < 0.05$, **: $P < 0.01$, ***: $P < 0.001$ relative to NaCl.

Figure 3. PET showed reduced uptake of [^{18}F]FLT 6 h after gemcitabine administration, and increased uptake after 1 d, whereas a growth inhibition related reduction in H1975 tumors could only be noted on d5. Static [^{18}F]FLT PET was performed at the indicated time points after gemcitabine treatment. Notably, for the 6 h time point, the tracer was injected about 4 h after drug administration. The PET image was acquired 70 - 90 min after tracer injection, during the 6th hour after drug application. Images show transverse slices at the biggest tumor diameter of one representative H1975 or A549 tumor over time. This longitudinal study did not include

the d5 time point. Hence, the images from d5 depict different tumors. Scale bar = 5 mm; white: NaCl; grey: gemcitabine; *: $P < 0.05$, **: $P < 0.01$, ***: $P < 0.001$ relative to NaCl; †: $P < 0.05$, ††: $P < 0.01$; †††: $P < 0.001$ relative to baseline.

Figure 4. Ki67 is unaltered after gemcitabine treatment. H1975 and A549 tumor sections were stained for Ki67 as described in materials and methods.. Scale bar = 100 μm; green: Ki67; blue: DAPI.

Figure 5. TK1 expression was correlated with [^{18}F]FLT uptake. Immunohistochemical analysis revealed a significant upregulation of TK1 1 d after administration of a single dose of gemcitabine in H1975 and A549 xenografts. Sections were stained in different batches, explaining the variations in color. Scale bar = 100 μM. There is a significant positive correlation of TK1 staining and [^{18}F]FLT uptake in both xenograft models (6 h values were omitted). **: $P < 0.01$ relative to NaCl.

Figure 6. Gemcitabine competed with [^{18}F]FLT *in vitro* and increased [^{18}F]FLT excretion and plasma thymidine levels after 6 h *in vivo*. (A) A549 cells were incubated with different concentrations of gemcitabine for 1 h or 4 h. Subsequently, [^{18}F]FLT uptake was determined either in the presence (+) or absence (-) of gemcitabine. Median values of n = 6 values, obtained in three different experiments, are displayed here. (B) Excretion of [^{18}F]FLT was assessed by calculating the tracer amount within the bladder relative to the radioactivity within the mouse. Data from mice bearing different tumor types were pooled. (C) Plasma and (D) tumor thymidine were quantified with an LC-MS/MS method. The plasma results from mice bearing different tumor types were pooled since the tumor appeared not to affect plasma thymidine

concentration. *: $P < 0.05$, **: $P < 0.01$, ***: $P < 0.001$ relative to NaCl; †: $P < 0.05$ relative to baseline.

Figure 7. ADC was not altered after gemcitabine therapy in H1975, which was in line with unchanged cellular density. (A) The ADC_{mean} of up to four transverse tumor sections was determined and averaged. (B) Cellular density was determined by counting DAPI positive nuclei in 20x fields of view (FOV: 580 µm x 460 µm) on Ki67 histology sections. White: NaCl; light grey: 1 d after gemcitabine; dark grey: 2 d after gemcitabine; Gem = gemcitabine; *: $P < 0.05$ relative to NaCl; †: $P < 0.05$, †††: $P < 0.005$ relative to baseline.
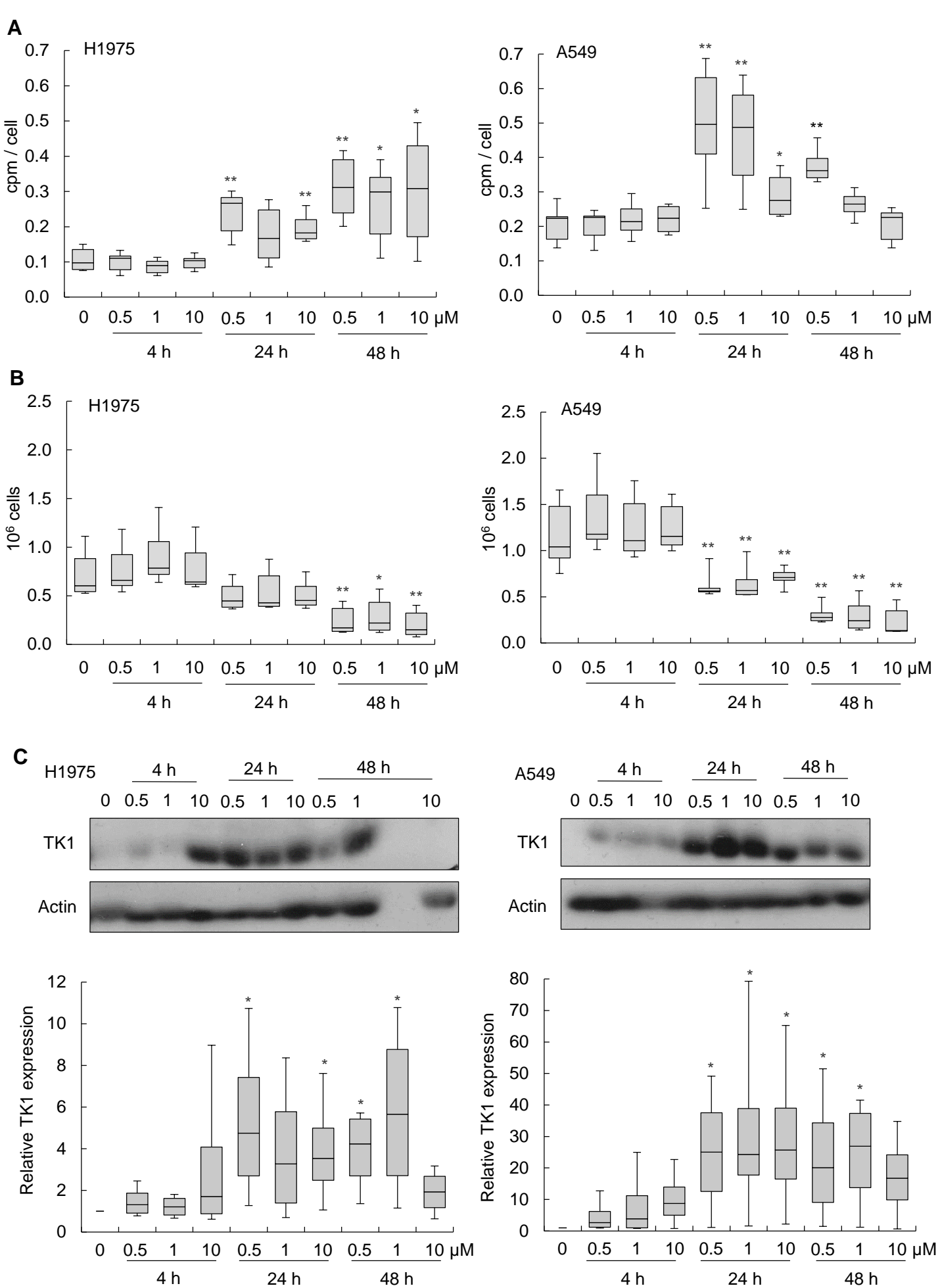
Figure 1
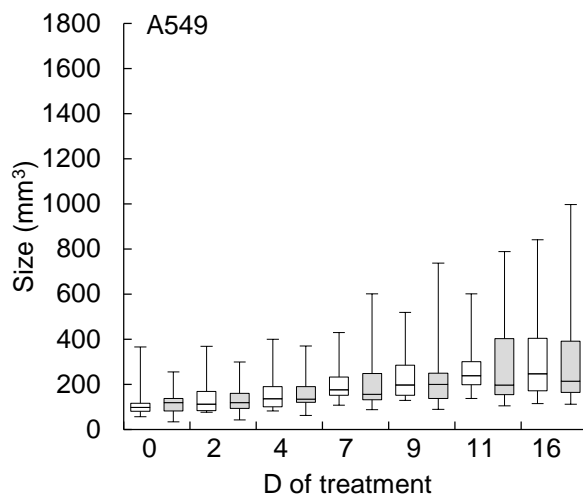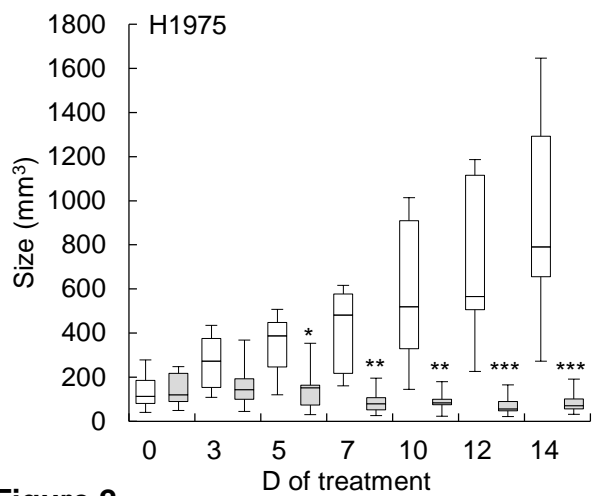
Figure 2
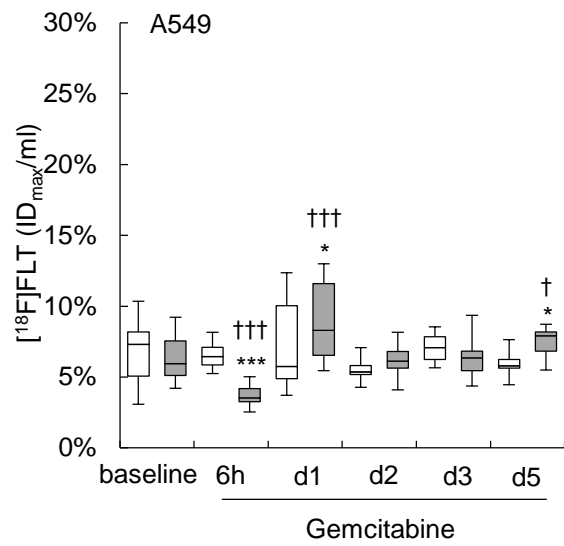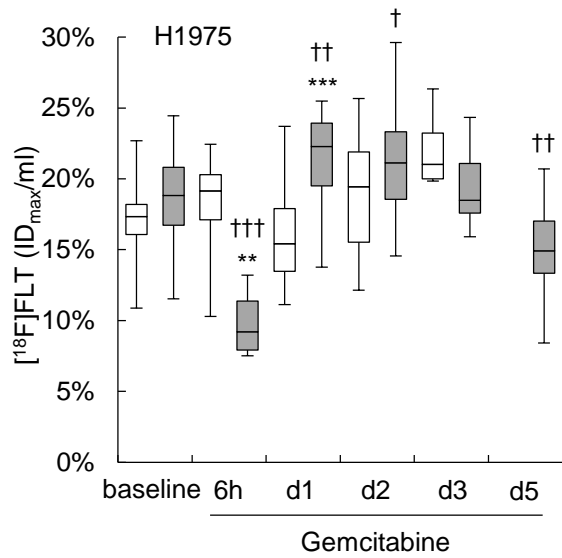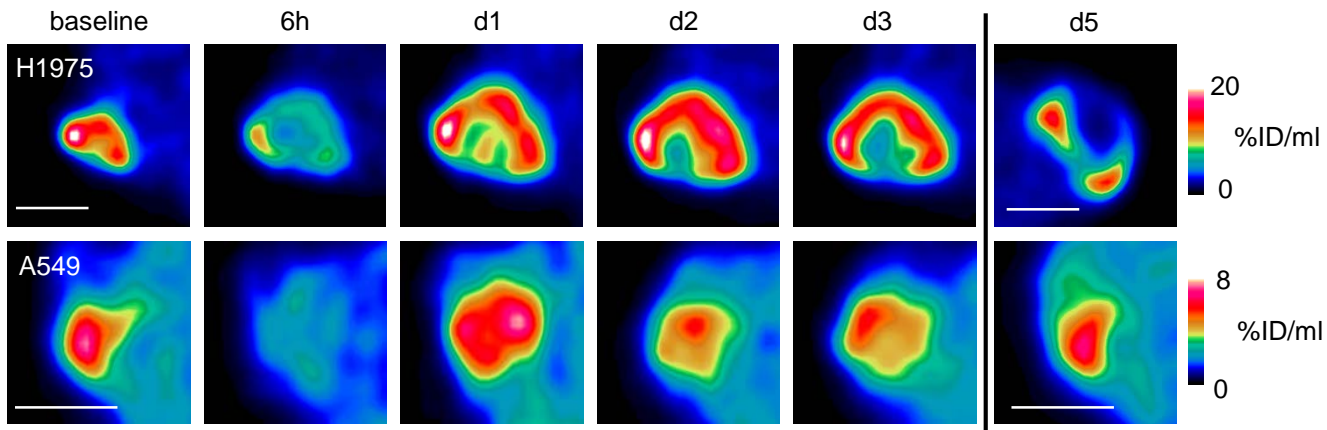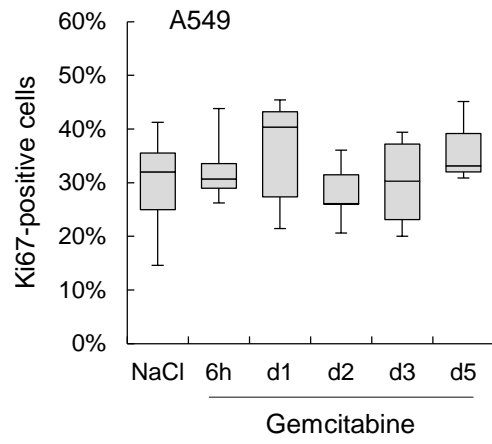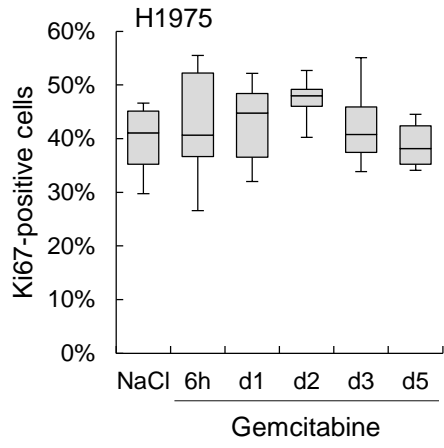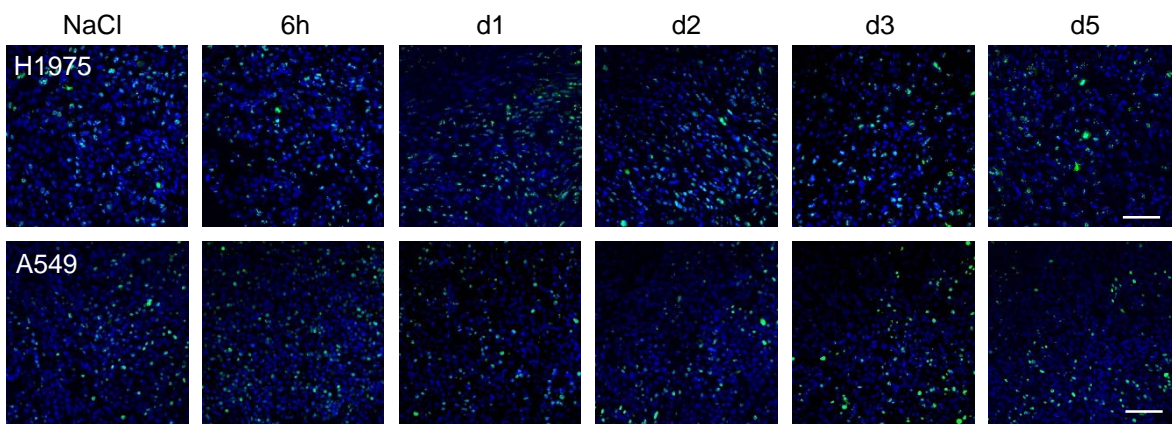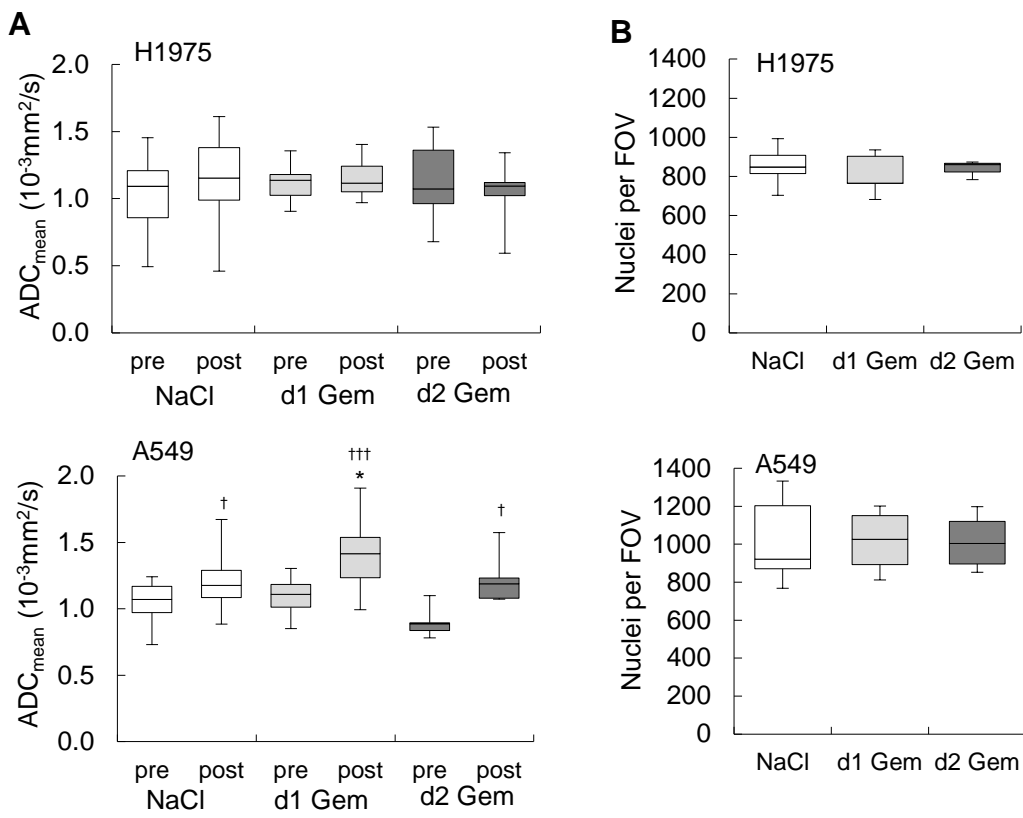
Figure 4
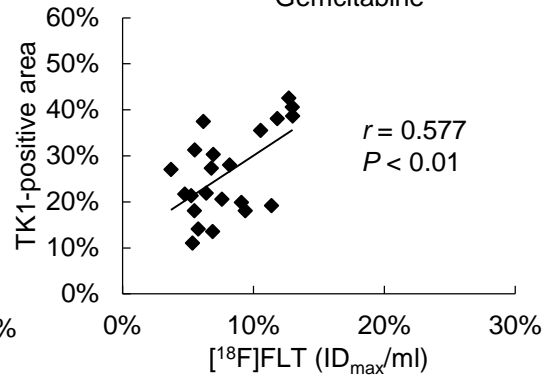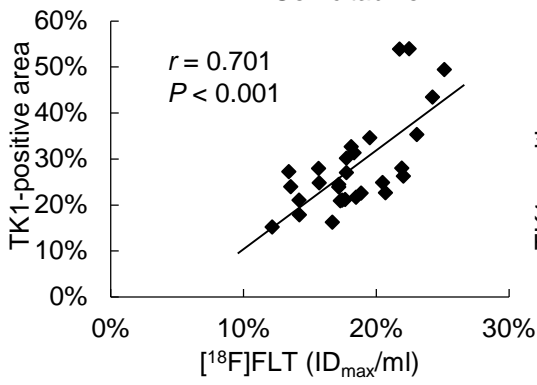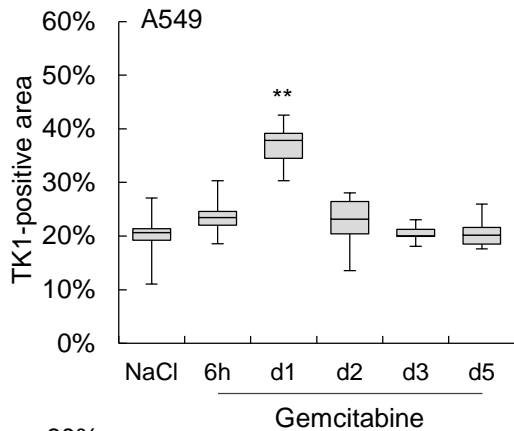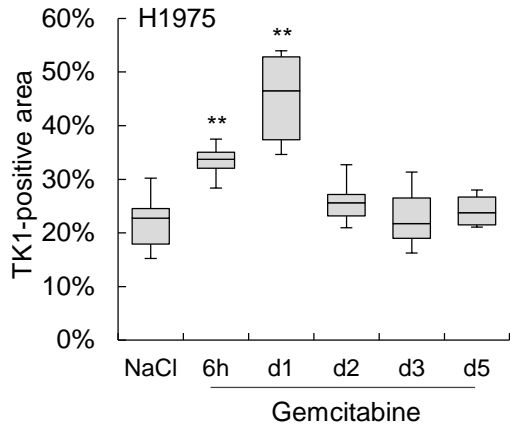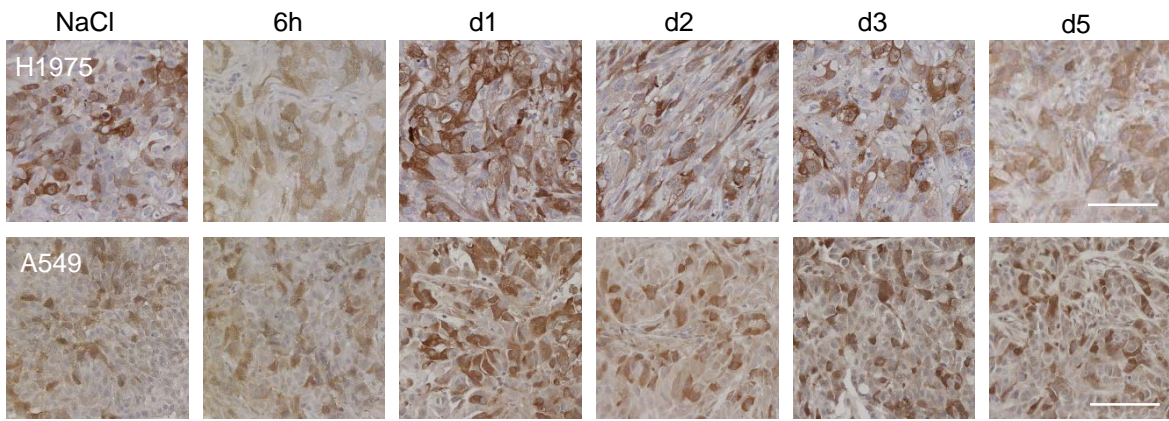
Figure 5
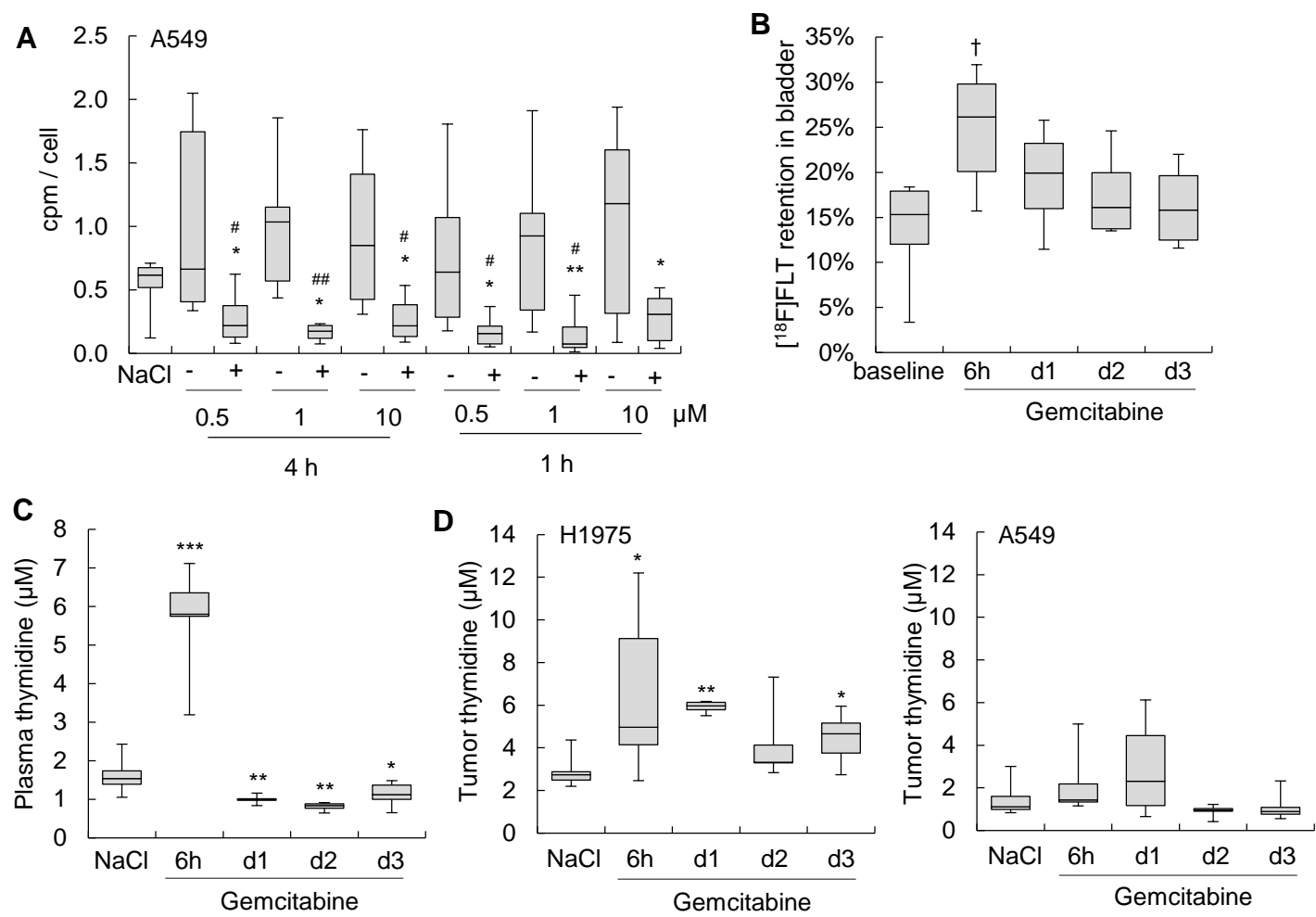
Figure 6

Figure 7

SUPPLEMENTARY FIGURE LEGENDS

Supplementary Figure S1. Outline of the experimental schedule pursued. This graphical demonstration depicts the number of animals imaged by [^{18}F]FLT PET and / or DW-MRI at the indicated time points. Seven imaging series were conducted per tumor model. Most animals were only imaged at a single time point after gemcitabine therapy, whereas subgroups were imaged repetitively. The cross indicates cervical dislocation of the animal and generation of samples for *ex vivo* analyses. The arrows indicate administration of NaCl / gemcitabine. *n* indicates the number of animals. Each animal was bearing up to three tumors in the shoulder region. Of note, not all samples available were analyzed. Number of samples included in analyses can be found in Supplementary Table S2.
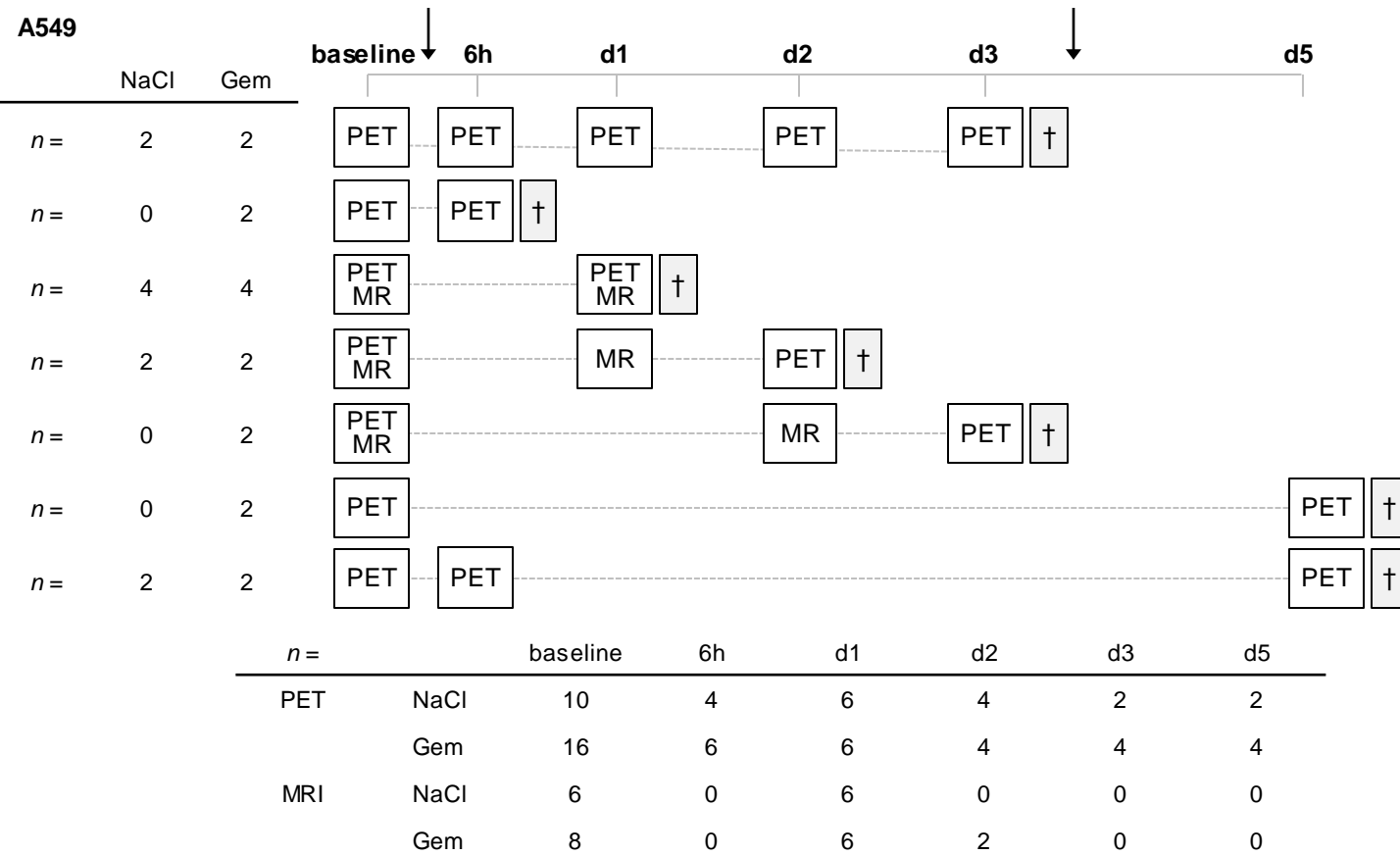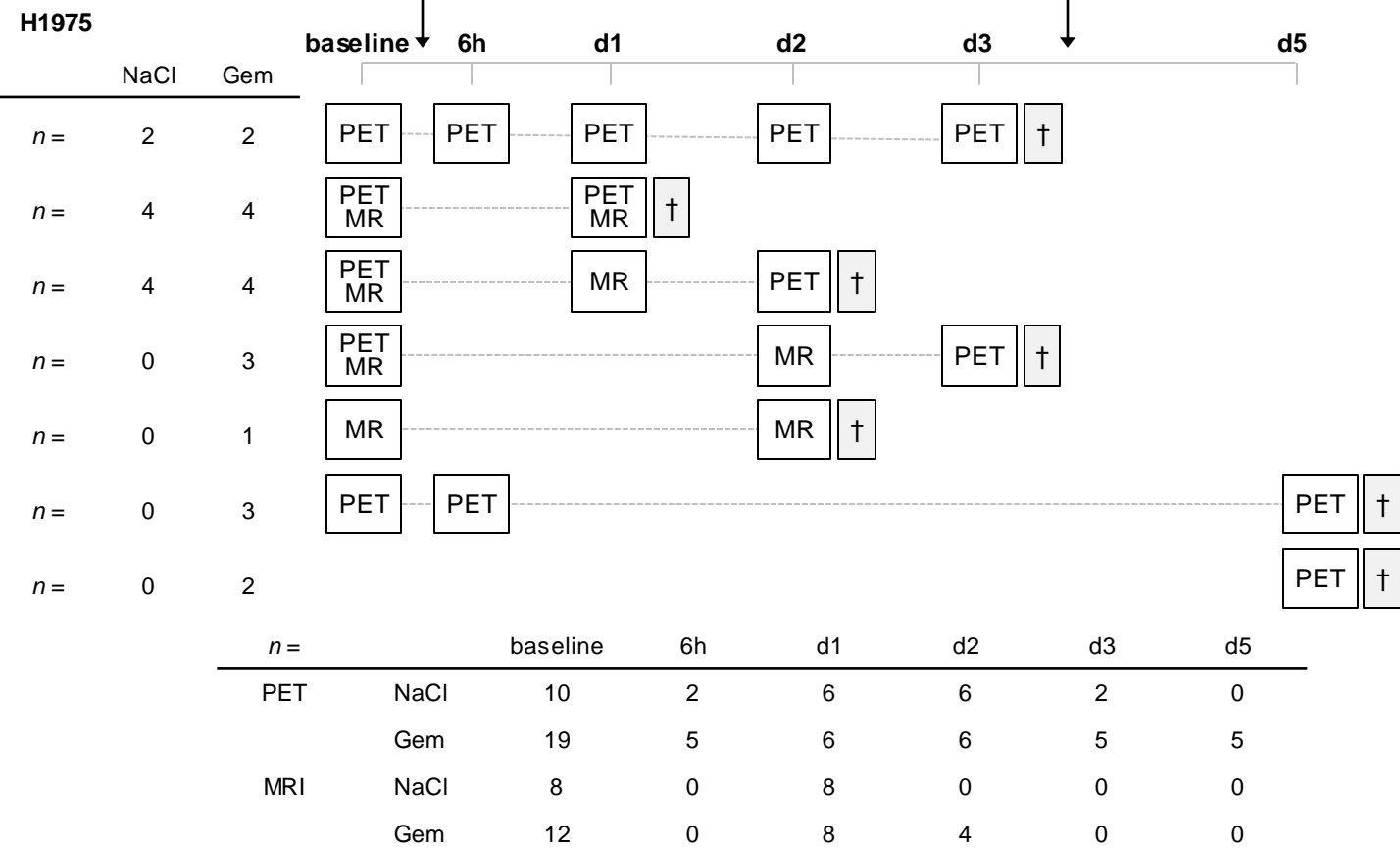
Supplementary Fig S2. Ki67 immunohistochemical staining. The merged microscopic images of Figure 4 are displayed as single channel images in grayscale. In the merged images, contrast and brightness of the single channels were adjusted (ImageJ) to show comparable staining intensities. This adjustment does not affect the quantification, since it does not affect the number of stained nuclei. Quantification was done on unprocessed images. The brightness of the single channel images was increased by 20 % (Power Point) to increase visibility of stained nuclei. Gem = gemcitabine; scale bar = 100 µm.

Supplementary Figure S3. TS and hENT1 expression are not altered 6 h after gemcitabine. Immunohistochemistry of hENT1 and TS was performed on *n* = 3 tumor samples per treatment condition. Immunohistochemistry was performed as described
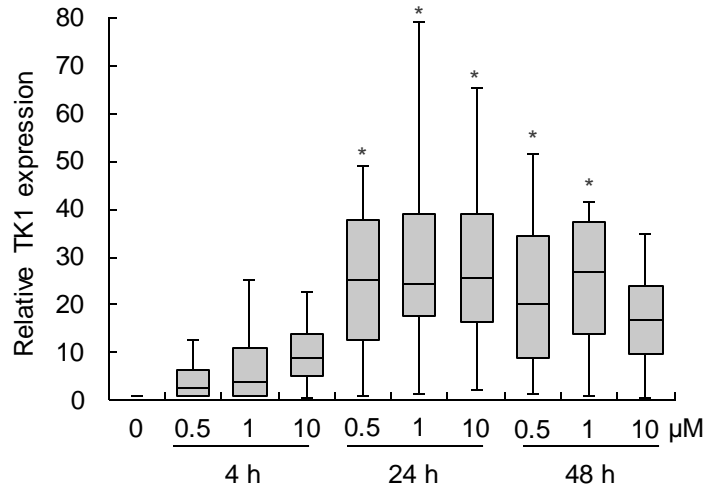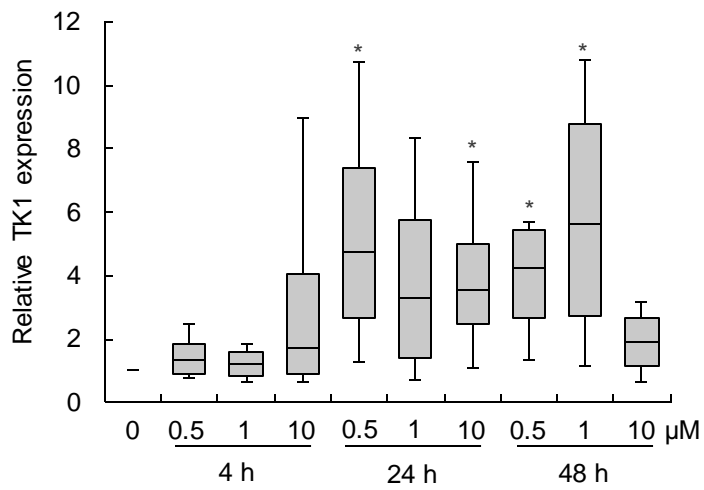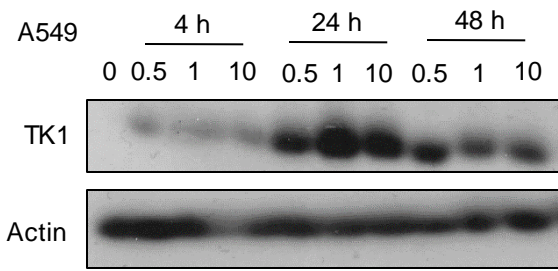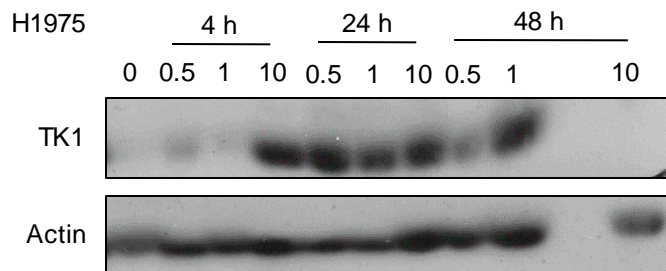
in Materials and Methods, using antibodies targeting TS (Abcam, ab108995, 1:50) or hENT1 (Acris, 11337-1-AP, 1:100). Brightness was increased by 20 % (PowerPoint) to increase visibility. scale bar = 100 µm.

Supplementary Figure S4. Gemcitabine induces increased apoptosis in H1975 tumors on d5. Immunohistochemistry was assessed from at least $n = 2$ tumors per condition, using an antibody targeting active caspase-3 (BD Pharmingen, CPP-32, Clone C92-605, 1:100). The stained area was significantly increased in H1975 on d5 (2.77 % ± 0.85 %) relative to NaCl treated tumors (0.72 % ± 0.33 %, $P < 0.001$, $n = 6$ each). scale bar = 100 µm.
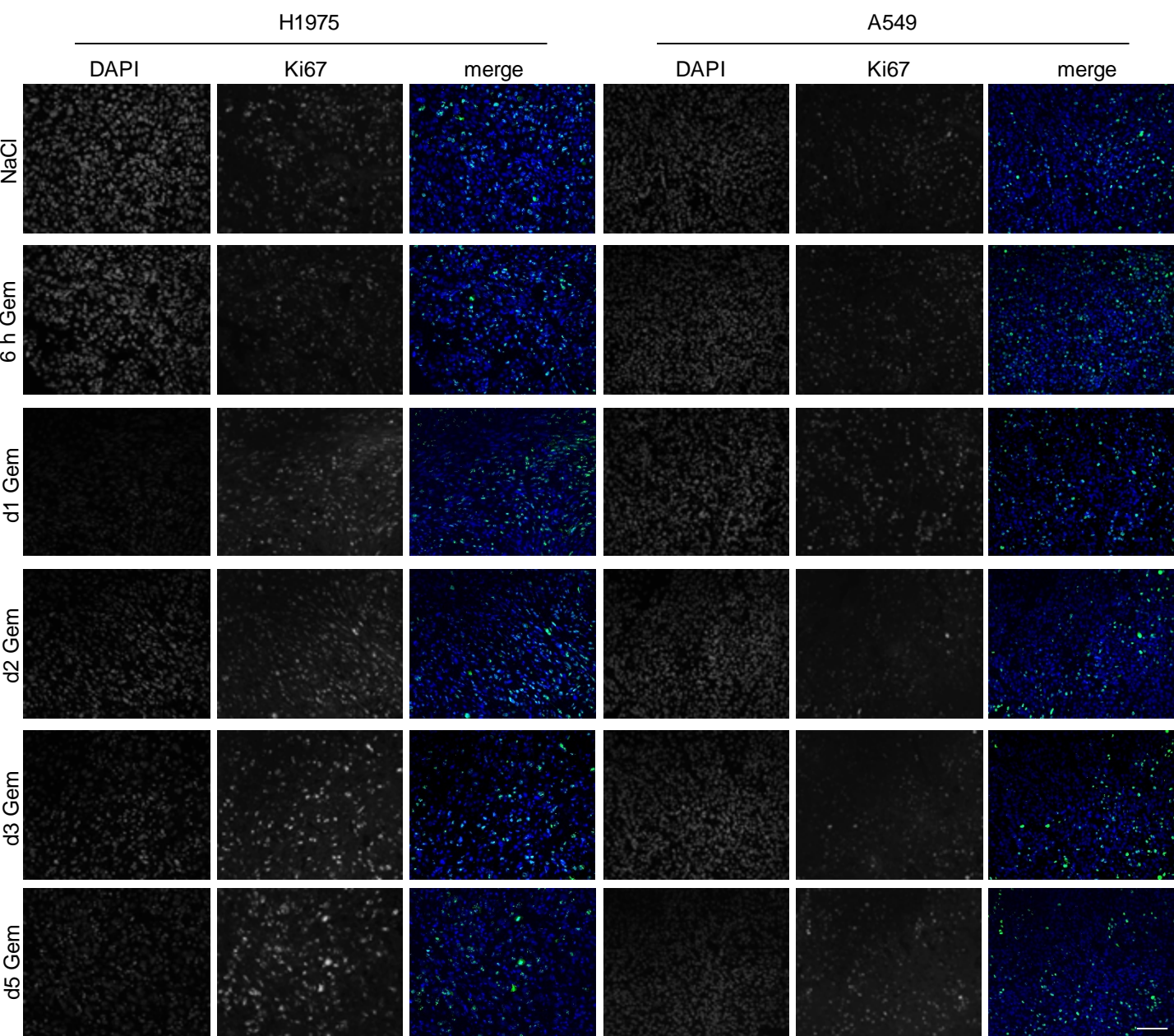
Supplementary Figure S5. 200 mg/kg gemcitabine affect growth of A549 xenografts. Mice bearing subcutaneous A549 xenografts were treated by intraperitoneal injections of 200 mg/kg gemcitabine in 3 d intervals (on d0, d3, d6 and d9). Caliper measurements revealed that this therapeutic regime is capable of inhibiting tumor growth relative to NaCl treated controls. See Supplementary Table S2 for absolute numbers and number of tumors. White: NaCl control; dark grey: 200 mg/kg gemcitabine; *: $P < 0.05$ relative to NaCl.
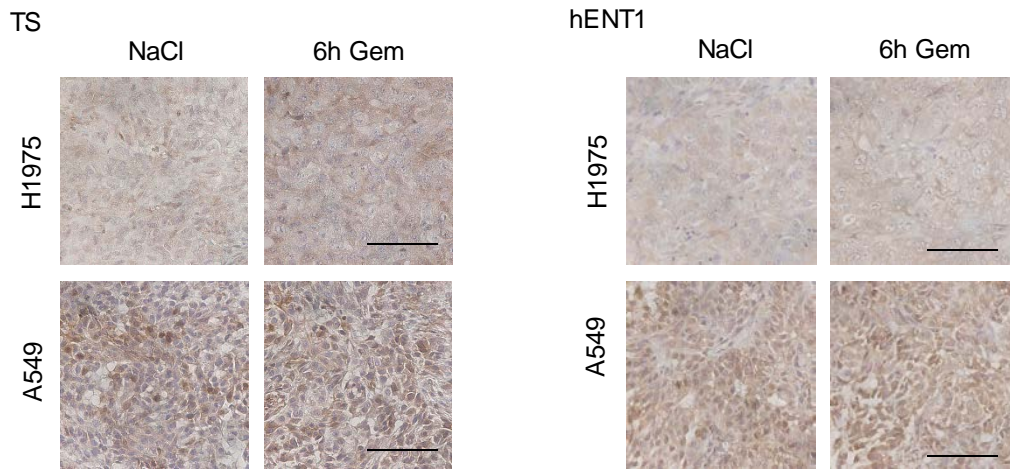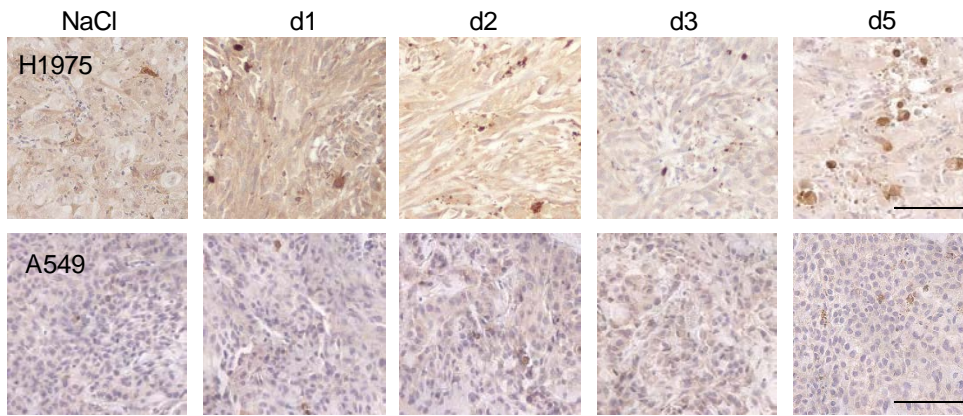
H1975

baseline　6h　d1　d2　d3　d5

	NaCl	Gem
n =	2	2
n =	4	4
n =	4	4
n =	0	3
n =	0	1
n =	0	3
n =	0	2

Timeline schematic: PET / MR / PET-MR imaging boxes with † markers across baseline, 6h, d1, d2, d3, d5.

n =		baseline	6h	d1	d2	d3	d5
PET	NaCl	10	2	6	6	2	0
	Gem	19	5	6	6	5	5
MRI	NaCl	8	0	8	0	0	0
	Gem	12	0	8	4	0	0

A549

baseline　6h　d1　d2　d3　d5

	NaCl	Gem
n =	2	2
n =	0	2
n =	4	4
n =	2	2
n =	0	2
n =	0	2
n =	2	2

Timeline schematic: PET / MR / PET-MR imaging boxes with † markers across baseline, 6h, d1, d2, d3, d5.

n =		baseline	6h	d1	d2	d3	d5
PET	NaCl	10	4	6	4	2	2
	Gem	16	6	6	4	4	4
MRI	NaCl	6	0	6	0	0	0
	Gem	8	0	6	2	0	0

Supplementary Figure S1

Supplementary Figure S2

Supplementary Figure S3

TS

	NaCl	6h Gem
H1975		
A549		

hENT1

	NaCl	6h Gem
H1975		
A549		

Supplementary Figure S4

	NaCl	d1	d2	d3	d5
H1975					
A549					

Supplementary Figure S5

Size (mm^3) vs D of treatment

Supplementary Figure S6

H1975		baseline	6 h	d1	d2	d3	d5
$\%ID_{mean}$/mL	NaCl	7.48 ± 1.52 (20)	6.18 ± 1.36 (5)	5.87 ± 1.24 (11)	6.94 ± 1.81 (14)	8.05 ± 1.26 (5)	
	Gem	7.56 ± 2.04 (38)	3.78 ± 0.64 (15) ††† **	7.83 ± 1.49 (17) **	8.79 ± 2.08 (16) † *	8.05 ± 1.60 (13)	4.85 ± 0.95 (10) †††
SUV_{max}	NaCl	5.25 ± 0.81 (20)	5.65 ± 1.51 (5)	4.99 ± 1.17 (14)	5.63 ± 1.30 (14)	6.70 ± 0.82 (5)	
	Gem	5.59 ± 0.98 (38)	2.88 ± 0.51 (15) ††† **	6.42 ± 0.91 (17) †† **	6.21 ± 1.13 (16)	5.90 ± 0.90 (13)	4.08 ± 1.05 (10) ††
SUV_{mean}	NaCl	2.27 ± 0.46 (20)	1.95 ± 0.42 (5)	1.84 ± 0.43 (12)	2.03 ± 0.53 (14)	2.44 ± 0.38 (5)	
	Gem	2.28 ± 0.62 (38)	1.12 ± 0.23 (15) ††† **	2.34 ± 0.45 (17) **	2.55 ± 0.58 (16) *	2.45 ± 0.50 (13)	1.32 ± 0.32 (10) †††
T-M	NaCl	6.59 ± 1.51 (20)	7.23 ± 1.83 (5)	5.66 ± 1.87 (14)	8.32 ± 1.88 (14)	10.15 ± 0.87 (5)	
	Gem	7.13 ± 1.61 (38)	4.73 ± 1.01 (15) ††† *	8.18 ± 1.92 (17) **	9.29 ± 1.46 (16) †††	9.96 ± 1.94 (13) †††	7.01 ± 1.76 (10)
T-L	NaCl	5.86 ± 1.30 (20)	6.73 ± 2.02 (5)	5.18 ± 1.83 (14)	7.47 ± 1.90 (14)	9.27 ± 0.78 (5)	
	Gem	6.26 ± 1.62 (38)	4.32 ± 0.99 (15) ††† *	7.28 ± 1.59 (17) † **	8.65 ± 1.99 (16) †††	8.67 ± 1.78 (13) †††	5.97 ± 1.78 (10)
25%ile	NaCl	12.3 ± 2.1 (20)	11.3 ± 2.6 (5)	9.2 ± 2.8 (14)	11.6 ± 3.1 (14)	14.1 ± 1.1 (5)	
	Gem	12.8 ± 2.9 (38)	6.2 ± 0.9 (15) ††† **	13.6 ± 2.1 (17) ***	14.8 ± 3.1 (16) † *	13.5 ± 2.2 (13)	8.5 ± 1.7 (10) †††

A549		baseline	6 h	d1	d2	d3	d5
$\%ID_{mean}$/mL	NaCl	3.58 ± 0.64 (27)	3.33 ± 0.30 (11)	3.81 ± 0.91 (16)	3.14 ± 0.35 (10)	3.67 ± 0.57 (5)	2.70 ± 0.17 (6)
	Gem	3.41 ± 0.50 (46)	2.12 ± 0.36 (18) ††† ***	4.06 ± 0.78 (18) ††	3.10 ± 0.40 (12)	2.99 ± 0.44 (11) †† *	3.36 ± 0.50 (11) *
SUV_{max}	NaCl	1.98 ± 0.56 (27)	1.95 ± 0.27 (11)	2.02 ± 0.74 (16)	1.66 ± 0.18 (10)	2.06 ± 0.27 (5)	1.77 ± 0.28 (6)
	Gem	1.97 ± 0.44 (46)	1.13 ± 0.23 (18) ††† ***	2.61 ± 0.72 (18) ††† *	1.99 ± 0.41 (12) *	1.96 ± 0.42 (11)	2.14 ± 0.26 (11) *
SUV_{mean}	NaCl	1.05 ± 0.19 (27)	1.00 ± 0.10 (11)	1.08 ± 0.21 (16)	0.95 ± 0.08 (10)	1.07 ± 0.12 (5)	0.80 ± 0.03 (6)
	Gem	1.05 ± 0.12 (46)	0.65 ± 0.13 (18) ††† ***	1.19 ± 0.19 (18) ††	1.01 ± 0.18 (12)	0.92 ± 0.11 (11) ††† *	0.95 ± 0.15 (11)
T-M	NaCl	2.50 ± 0.63 (27)	2.74 ± 0.44 (11)	2.52 ± 1.03 (16)	2.31 ± 0.20 (10)	2.78 ± 0.26 (5)	2.67 ± 0.42 (6)
	Gem	2.58 ± 0.70 (46)	1.95 ± 0.22 (18) ††† ***	3.66 ± 1.09 (18) ††† **	3.01 ± 0.49 (12) † **	3.05 ± 0.63 (11) †	3.59 ± 0.42 (11) ††† **
T-L	NaCl	2.18 ± 0.63 (27)	2.33 ± 0.37 (11)	2.18 ± 0.92 (16)	1.95 ± 0.18 (10)	2.31 ± 0.18 (5)	2.26 ± 0.35 (6)
	Gem	2.19 ± 0.55 (46)	1.58 ± 0.18 (18) ††† ***	3.01 ± 0.81 (18) ††† **	2.55 ± 0.47 (12) † **	2.79 ± 0.68 (11) ††	3.11 ± 0.37 (11) ††† **
25%ile	NaCl	5.01 ± 1.10 (27)	4.80 ± 0.42 (11)	5.32 ± 1.69 (16)	4.30 ± 0.45 (10)	5.16 ± 0.83 (5)	3.99 ± 0.35 (6)
	Gem	4.73 ± 0.80 (46)	2.82 ± 0.45 (18) ††† ***	6.16 ± 1.37 (18) †††	4.43 ± 0.56 (12)	4.28 ± 0.65 (11)	4.83 ± 0.69 (11) *

Supplementary Table S2. Mean and standard deviation, as well as number of samples analyzed (in brackets), of the data presented in this article. *: $P < 0.05$, **: $P < 0.01$, ***: $P < 0.001$ relative to NaCl; †: $P < 0.05$, ††: $P < 0.01$, †††: $P < 0.001$ relative to baseline; #: $P < 0.05$, ##: $P < 0.01$ relative to respective "+ Gem" sample (Mann-Whitney Rank Sum Test). Gem = gemcitabine.

Fig. 1. [18F]FLT uptake assay after incubation with NaCl / gemcitabine

		H1975			A549		
		10³ cpm	10³cells	cpm / cell	10³ cpm	10³cells	cpm / cell
NaCl		75 ± 25	723 ± 25	0.11 ± 0.03	225 ± 28	1,166 ± 380	0.21 ± 0.06
0.5 µM	4h	79 ± 37	774 ± 259	0.10 ± 0.03	264 ± 21 *	1,378 ± 419	0.20 ± 0.05
	24h	122 ± 62	498 ± 148	0.24 ± 0.07 **	293 ± 63	621 ± 145 **	0.50 ± 0.17 **
	48h	75 ± 48	244 ± 150 **	0.31 ± 0.09 **	117 ± 43 **	308 ± 100 **	0.38 ± 0.05 **
1 µM	4h	79 ± 30	910 ± 301	0.09 ± 0.02	265 ± 44	1,252 ± 353	0.22 ± 0.05
	24h	84 ± 17	549 ± 223	0.18 ± 0.08	279 ± 58	647 ± 184 **	0.46 ± 0.16 **
	48h	78 ± 64	293 ± 193 *	0.27 ± 0.11 *	74 ± 36 **	297 ± 173 **	0.26 ± 0.04
10 µM	4h	80 ± 37	789 ± 264	0.10 ± 0.02	270 ± 19 **	1,256 ± 268	0.22 ± 0.04
	24h	97 ± 24	509 ± 149	0.20 ± 0.04 **	202 ± 32	710 ± 100 **	0.29 ± 0.06 *
	48h	77 ± 85	208 ± 144 **	0.30 ± 0.16 *	41 ± 16 **	235 ± 163 **	0.20 ± 0.05

Fig. 2 / Supplementary Fig. S2. Growth of lung cancer xenografts upon gemcitabine therapy

		d0	d3	d5	d7	d10	d12	d14
A) H1975	NaCl	138 ± 84 (7)	267 ± 133 (7)	343 ± 143 (7)	407 ± 201 (7)	594 ± 352 (7)	746 ± 385 (7)	944 ± 507 (7)
	100 mg/kg	147 ± 79 (7)	163 ± 106 (7)	144 ± 106 (7) *	88 ± 56 (7) **	91 ± 47 (7) **	74 ± 47 (7) ***	87 ± 53 (7) ***
B) A549	NaCl	121 ± 77 (16)	139 ± 76 (16)	168 ± 96 (16)	207 ± 86 (16)	243 ± 120 (16)	283 ± 136 (16)	301 ± 196 (13)
	100 mg/kg	118 ± 53 (17)	134 ± 67 (17)	169 ± 87 (17)	210 ± 131 (16)	235 ± 162 (17)	277 ± 180 (17)	312 ± 223 (17)
	200 mg/kg	108 ± 107 (6)	95 ± 104 (6)	119 ± 129 (6)	118 ± 126 (6) *	146 ± 175 (6) *	172 ± 197 (6) *	225 ± 273 (6)

Fig. 3. [18F]FLT uptake in gemcitabine treated xenografts (%ID$_{max}$/mL)

		baseline	6 h	d1	d2	d3	d5
H1975	NaCl	17.3 ± 2.6 (20)	17.9 ± 4.6 (5)	15.7 ± 3.6 (14)	19.3 ± 4.5 (14)	22.1 ± 2.7 (5)	n.d.
	Gem	18.6 ± 3.3 (38)	9.8 ± 2.0 (15) ††† **	21.5 ± 3.2 (17) †† ***	21.4 ± 4.1 (16) †	19.4 ± 2.7 (13)	15.0 ± 3.4 (10) ††
A549	NaCl	6.73 ± 1.92 (27)	6.52 ± 0.88 (11)	7.15 ± 2.93 (16)	5.49 ± 0.74 (10)	7.07 ± 1.17 (5)	5.94 ± 1.04 (6)
	Gem	6.39 ± 1.57 (46)	3.68 ± 0.68 (18) ††† ***	8.95 ± 2.75 (18) ††† *	6.12 ± 1.04 (12)	6.41 ± 1.59 (11)	7.55 ± 1.03 (11) † *

Fig. 4. Ki67 staining (% positive nuclei)

	NaCl	6 h Gem	d1 Gem	d2 Gem	d3 Gem	d5 Gem
H1975	39.4 ± 6.0 (9)	42.3 ± 11.8 (5)	42.9 ± 8.1 (6)	47.2 ± 5.1 (4)	42.6 ± 9.1 (4)	38.8 ± 4.4 (6)
A549	30.2 ± 8.4 (11)	32.4 ± 6.2 (6)	35.8 ± 10.5 (6)	28.1 ± 5.9 (5)	30.0 ± 9.4 (4)	36.4 ± 7.7 (3)

Fig. 5. TK1 staining (% positive area)

	NaCl	6 h Gem	d1 Gem	d2 Gem	d3 Gem	d5 Gem
H1975	22.1 ± 4.9 (13)	33.3 ± 3.8 (4) **	45.1 ± 8.8 (6) ***	25.8 ± 4.1 (6)	23.1 ± 7.6 (3)	24.2 ± 3.0 (6)
A549	19.9 ± 5.8 (5)	23.6 ± 3.6 (7)	36.8 ± 4.3 (8) **	22.3 ± 5.6 (8)	20.5 ± 1.6 (7)	20.7 ± 3.1 (6)

Fig. 6. *In vitro* competition assay (cpm / cell)

preincubation with	0.5 µM Gem		1 µM Gem		10 µM Gem	
[18F]FLT uptake	- Gem	+ Gem	- Gem	+ Gem	- Gem	+ Gem
NaCl	0.53 ± 0.22					
4h preincubation	1.02 ± 0.81	0.28 ± 0.21 # *	0.99 ± 0.53	0.17 ± 0.07 ## *	0.94 ± 0.61	0.27 ± 0.18 # *
1h preincubation	0.77 ± 0.63	0.17 ± 0.12 # *	0.87 ± 0.66	0.15 ± 0.17 # **	1.03 ± 0.79	0.28 ± 0.20 *

Fig. 6B. [18F]FLT uptake in bladder

	NaCl	6 h Gem	d1 Gem	d2 Gem	d3 Gem
% of total	13.7 ± 5.8 (6)	24.8 ± 6.5 (6) †	19.3 ± 6.2 (4)	17.6 ± 5.2 (4)	16.3 ± 4.9 (4)

Fig. 6C-D. Thymidine concentrations (µM)

	NaCl	6 h Gem	d1 Gem	d2 Gem	d3 Gem
B) plasma	1.64 ± 0.45 (10)	5.76 ± 1.24 (7) ***	0.99 ± 0.10 (6) **	0.81 ± 0.12 (4) **	1.13 ± 0.33 (5) *
C) H1975	2.90 ± 0.77 (6)	6.39 ± 3.41 (10) *	5.91 ± 0.28 (5) **	4.18 ± 1.82 (5)	4.47 ± 1.17 (6) *
D) A549	1.39 ± 0.66 (10)	2.06 ± 1.25 (9)	2.86 ± 1.94 (12)	0.92 ± 0.27 (6)	1.09 ± 0.64 (6)

Fig. 7A. ADC$_{mean}$ (10^{-3}/mm²)

	NaCl		d1 Gem		d2 Gem	
	pre	post	pre	post	pre	post
H1975	1.029 ± 0.260 (23)	1.186 ± 0.203 (20)	1.096 ± 0.192 (20)	1.133 ± 0.152 (20)	1.147 ± 0.252 (8)	1.058 ± 0.196 (10)
A549	1.044 ± 0.163 (16)	1.196 ± 0.198 (14) †	1.096 ± 0.127 (13)	1.400 ± 0.227 (18) ††† *	0.900 ± 0.121 (5)	1.229 ± 0.204 (5) †

Fig. 7B. Nuclei per field of view

	NaCl	d1 Gem	d2 Gem
H1975	858 ± 93 (9)	810 ± 106 (5)	839 ± 49 (3)
A549	1031 ± 211 (11)	1018 ± 163 (6)	1014 ± 160 (4)

Supplementary Table S3. Mean and standard deviation, as well as number of samples analyzed (in brackets), of [^{18}F]FLT uptake in organs other than the tumor 6 h after gemcitabine (%ID$_{max}$/mL). *: $P < 0.05$ relative to NaCl; $\dagger\dagger$: $P < 0.01$ relative to baseline.

	baseline	6h Gem
liver	3.97 ± 0.56 (27)	3.25 ± 0.49 (6)
muscle	3.50 ± 0.46 (27)	2.79 ± 0.33 (6) $\dagger\dagger$ *
sternum	3.61 ± 1.03 (27)	2.66 ± 0.46 (6) $\dagger\dagger$
femur	3.52 ± 0.59 (27)	3.22 ± 0.39 (6)
spleen	3.86 ± 0.56 (27)	2.73 ± 0.41 (6) $\dagger\dagger$ *
axillary lymph node	3.05 ± 0.41 (25)	2.25 ± 0.60 (6) $\dagger\dagger$